Ther Adv Neurol Disord

2019, Vol. 12: 1–9

DOI: 10.1177/1756286419843040

First *in vivo* visualization of the human subarachnoid space and brain cortex via optical coherence tomography

Karl Hartmann, Klaus-Peter Stein, Belal Neyazi and Ibrahim Erol Sandalcioglu

Abstract: The present work explores optical coherence tomography (OCT) as a suitable *in vivo* neuroimaging modality of the subarachnoid space (SAS). Patients ($n = 26$) with frontolateral craniotomy were recruited. The temporal and frontal arachnoid mater and adjacent anatomical structures were scanned using microscope-integrated three-dimensional OCT, (iOCT). Analysis revealed a detailed depiction of the SAS (76.9%) with delineation of the internal microanatomical structures such as the arachnoid barrier cell membrane (ABCM; 96.2%), trabecular system (50.2%), internal blood vessels (96.2%), pia mater (26.9%) and the brain cortex (96.2%). Orthogonal distance measuring was possible. The SAS showed a mean depth of 570 µm frontotemporal. The ABCM showed a mean depth of 74 µm frontotemporal. These results indicate that OCT provides a dynamic, non-invasive tool for real-time imaging of the SAS and adjacent anatomical structures at micrometer spatial resolution. Further studies are necessary to evaluate the value of OCT during microsurgical procedures.

Keywords: intraoperative imaging, optical coherence tomography, subarachnoid space, trabecular system

Received: 14 November 2018; revised manuscript accepted: 10 March 2019

Introduction

The subarachnoid space (SAS) is the cavity between the arachnoid barrier cell membrane (ABCM) and the pia mater, filled with cerebrospinal fluid (CSF). The microstructural composition is considered a basis for the understanding of physiological and further pathophysiological functions of the brain.[1] Although representing the largest continuous intrathekal compartment, the SAS of the cerebral convexity, in particular, hides from *in vivo* visualization due to technical limitations. Conventional imaging tools like magnetic resonance imaging (MRI) and ultrasound (US) - currently the most established tool for dynamic sectional imaging of the brain - are llmited here due to their lack of spatial resolution.[2–4]

In contrast, optical coherence tomography (OCT) shows an exceedingly high maximal spatial resolution of 1–15 µm, which approaches the resolution of conventional histopathology.[5] OCT imaging depends on the detection of back scattered near-infrared light. It is harmless to biological tissue.[6] Due to these physical properties light microscope integration is possible. Therefore, immediate three-dimensional (3D), sectional scanning of tissue during microsurgical procedures is feasible. Medical applications already span the fields of neurology, cardiology, dermatology and ophthalmology.[7–10] In ophthalmology it is regularly implemented in vitro-retinal surgical setups.[11]

In neuroimaging polarization sensitive OCT has proven its potential for delineation of white and grey matter in rat brain[12] and fibre tracts in the human brain in post mortem conditions.[13] In the field of neurosurgery, OCT could be used as a device for 'optic biopsy'.[14,15] *Ex vivo* solid tumors, diffusely invaded brain tissue and the normal brain in human gliomas could be differentiated.[16] *In vivo*, during glioma surgery, residual tumors could be depicted in the mouse[17] and human brain.[18]

Correspondence to:
Karl Hartmann
Department of Neurosurgery, KRH Klinikum Nordstadt, Haltenhoffstraße 41, Hanover 30167, Germany
karl.hartmann@krh.eu

Klaus-Peter Stein
Belal Neyazi
Ibrahim Erol Sandalcioglu
Department of Neurosurgery, KRH Klinikum Nordstadt, Hanover, Germany

Ex vivo, in a porcine brain with released CSF, OCT imaging could delineate the sulcal arachnoid trabeculae and arachnoid blood vessels,[19] but the study could not depict intact sulcal or gyral SAS.

Due to light translucent tissue properties in combination with a penetrating depth of 4000 µm and suitable spatial resolution[20] we hypothesized that OCT is a useful tool for the visualization of the microstructural composition of the human SAS *in vivo*.

Materials and methods

Participants

Patients (n = 26; female = 13, male = 13) with indication for frontolateral craniotomy were included. Diagnoses ranged from intracranial tumors (n = 13), unruptured cerebral aneurysms (n = 11) and arteriovenous malformations (n = 2). Patients were positioned supine or semi-supine. The study was approved by the local ethics committee (no. 3012-2016). All participants gave written informed consent.

Optical coherence tomography

Intraoperative OCT was enabled by connecting the OCT camera (OptoMedical Technologies GmbH, Lübeck, Germany) to the port of a surgical microscope optimized for light transmission in the near-infrared spectral range (HS Hi-R1000G, Haag-Streit Surgical GmbH, Wedel, Germany). OCT scanning was displayed on internal and external monitors as well as a transparent overlay in the field of view of the surgeon (head-up display). OCT volume scans and corresponding light microscopic pictures were further stored for post-procedural analysis. The OCT camera was optimized for the optics of the operating microscope. The scan head of the OCT device was connected with an optical light fibre cable and electronic cable to the OCT camera head. The OCT camera consisted of a light source at a central wavelength of 840 nm with a spectral bandwidth of 55 nm, a spectral domain detector with a speed of 15,000 A-scans/second. The detector speed resulted in an OCT speed of 10 frames/second. A two-axis scanner enabled 3D volume scans. Internal motorized reference optics allowed for different working distances ranging from 200 to 480 mm. The optical window depth was 4.2 mm in air and approximately 3.1 mm in brain tissue with an index of refraction of 1.34. The measured axial spatial resolution was approximately 10 µm in air and approximately 7.5 µm in tissue. The lateral scan width depended on the magnification of the microscope and varied from 5 mm up to 37 mm. The lateral resolution ranged from 23 µm up to 47 µm at a working distance of 232 mm depending on the microscope magnification. The system was CE certified (conformity with the European Union guidelines) for intraoperative documentation of tissue structures. For a detailed description, see Gallwas and colleagues.[21] The OCT setting is demonstrated in Figure 1.

Image acquisition

The region of interest (ROI) was defined by the surgeon, according to the surgical approach. A rectangular scan angle to the surface of the ROI and the highest microscope magnification was intended. For each ROI the corresponding light microscopic picture and 3D OCT volume scan were recorded and stored with a data sheet defining: the date and time of scanning, scan angle, number of A-scans, number of B-scans, height in pixels, ranges of volume scan in mm, zoom of microscope and focus of microscope.

Anatomical analysis and distance measurements

Microscopic pictures of the scanned site and corresponding OCT volume scans were sorted according to image quality and richness of anatomical details. The aspect ratio of the selected OCT scans was adjusted according to the microscope magnification. For anatomical analysis the data sets were then screened by two independent neurosurgeons with experience in OCT imaging. For distance measurement an exemplary A-scan was selected from the volume scan. A rectangular measurement angle parallel to the optic path and measurement under maximum augmentation was maintained in any case. Whenever feasible, the center of the probe was selected to reduce scattering effects. The final measurement site was marked. All steps were done using ImageJ2 and Fiji software.[22,23] Measuring was not adjusted according to the index of refraction.

Results

Anatomical structures of the SAS

A detailed depiction of the microanatomical structures of the SAS and adjacent brain tissue

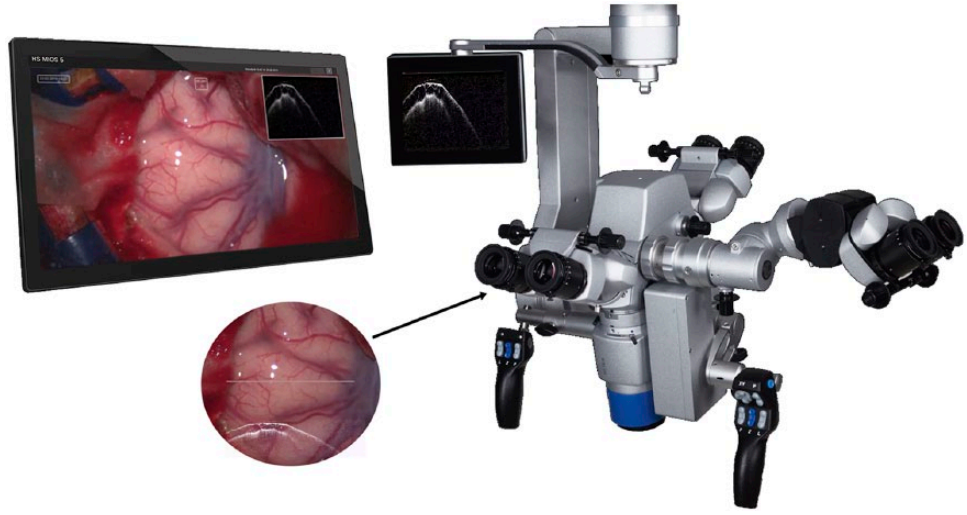

Figure 1. The OCT-camera (OptoMedical Technologies GmbH, Lübeck, Germany) is connected to the port of a surgical microscope (HS Hi-R1000G, Haag-Streit Surgical GmbH, Wedel, Germany), which is optimized for light transmission in near-infrared spectral range. OCT scanning is displayed on internal and external monitors and as a transparent overlay in the field of view of the surgeons (head-up display). Photograph with permission of OptoMedical.
iOCT, microscope-integrated three-dimensional OCT.

Table 1. Screening of anatomical structures.

	Volume scans		CSF *in situ*		CSF *released*	
	n	%	*n*	%	*n*	%
Cases	26		12	46.2%	14	53.9%
SAS	20	76.9%	12	100.0%	12	85.7%
ABCM	25	96.2%	11	91.7%	0	0.0%
Trabecular system	13	50.2%	13	66.7%	9	60%
Blood vessels	25	96.2%	12	100.0%	12	85.7%
Pia mater	7	26.9%	3	25.0%	4	26.7%
Brain cortex	25	96.2%	11	91.7%	14	93.3%

Number of volume scans in which the corresponding anatomical structure could be delineated overall, before and after CSF release and percentage share. In CSF-released cases the perivascular SAS was screened.
ABCM, arachnoid barrier cell membrane; CSF, cerebrospinal fluid; SAS, subarachnoid space.

was possible in most of the volume scans. The SAS (76.9%), ABCM (96.2%), trabecular system (66.7%), internal blood vessels (96.2%), pia mater (26.9%) and the brain cortex (96.2%) could be delineated, (Table 1, Figure 2; see supplemental material for 3D volume scan of the frontal SAS, S1).

When the CSF was released microanatomical structures could still be depicted but were less detailed. The perivascular and gyral SAS (85.7%), trabecular system (60%), internal blood vessels (85.7%), pia mater (26.7%) and the brain cortex (93.33%) could be delineated. The ABCM (0%) could not be delineated, since a clear differentiation to the underlying trabecular system (60%) was not given (Figure 3, Table 1).

OCT scanning showed that subarachnoid haemorrhage (SAH) could be depicted (Figure 4).

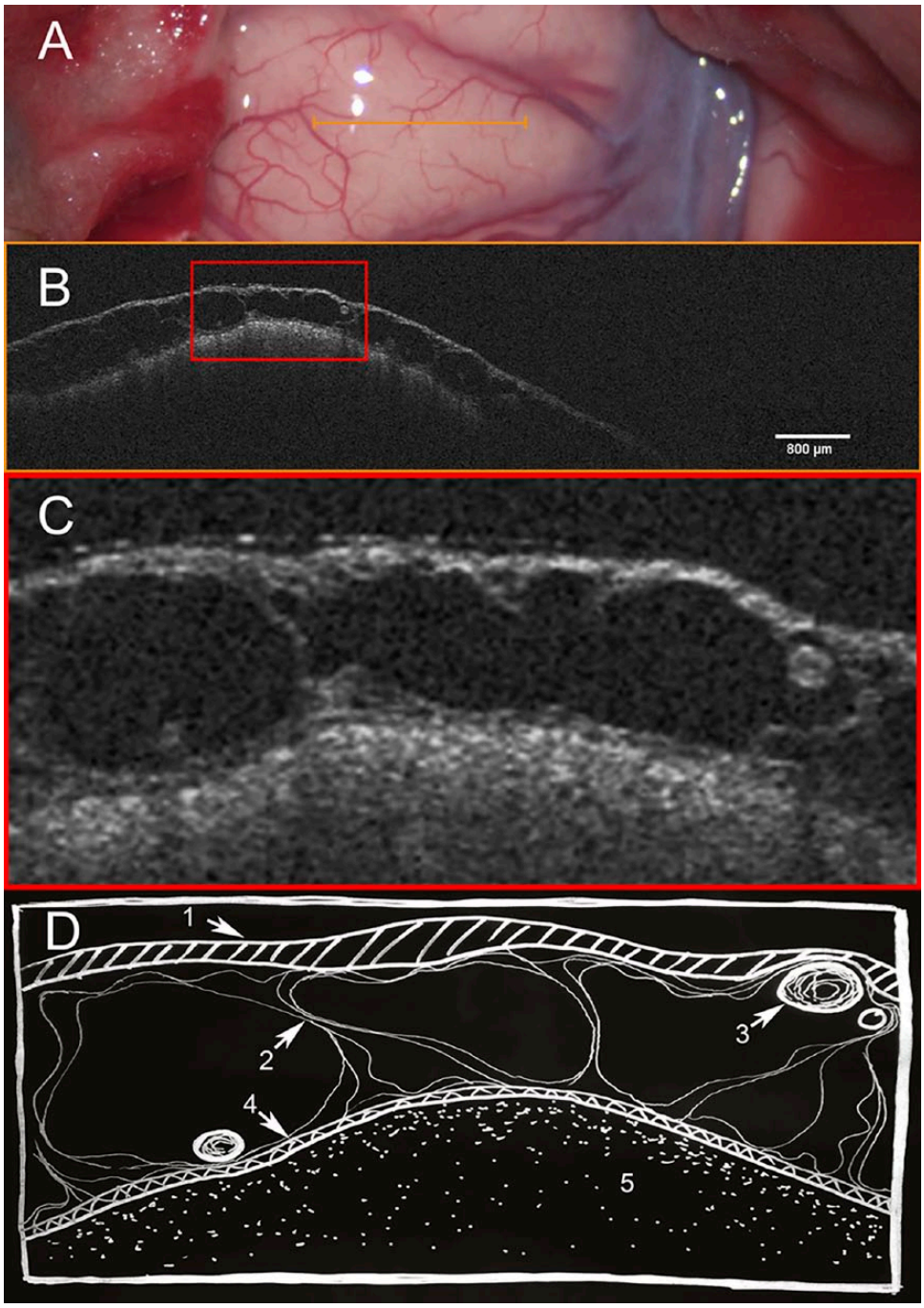

Figure 2. Microscopic view of the frontal lobe and sylvian fissure. Orange line indicates the region of scan. B: OCT-scan of the region depicting the gyral SAS. C: Enlarged excerpt demonstrating details of the SAS. D: Schematic drawing of microstructures: 1. ABCM, 2. Trabecular system, 3. Internal blood vessels, 4. Pia mater and 5. Brain cortex.
CSF, cerebrospinal fluid; OCT, optical coherence tomography; SAS, subarachnoid space.

Orthogonal distance measurement of the SAS and ABCM

Orthogonal distance measuring was possible. The gyral SAS showed a mean depth of 570 µm frontotemporal, 463 µm frontal and 676 µm temporal. The sylvian SAS showed, as anatomically expected, a higher mean depth of 1204 µm. See Figure 5 for the measurement technique and Figure 6 for the values of the frontal and temporal SAS depth.

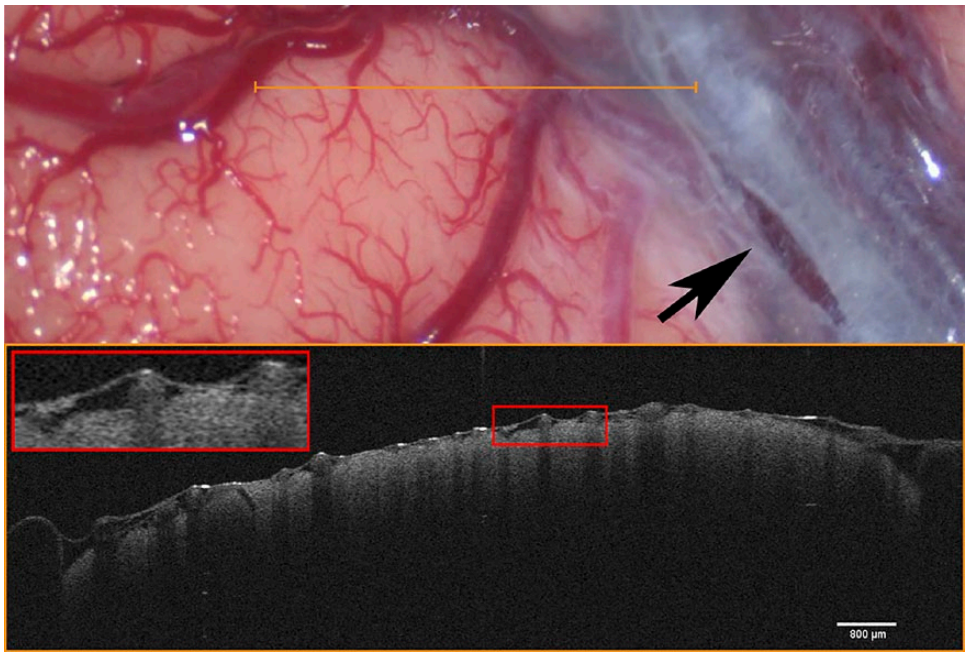

Figure 3. Above light microscopic view of the frontal lobe after CSF release. The orange line indicates the site of OCT-scan. The black arrow demonstrates the site of CSF release - suprasylvian incision of the ABCM. Below OCT-scan of the region visualizing the collapsed SAS, with adjacent internal blood vessels. Red rectangle shows enlarged details of the OCT-Scan.
CSF, cerebrospinal fluid; OCT, optical coherence tomography; SAS, subarachnoid space.

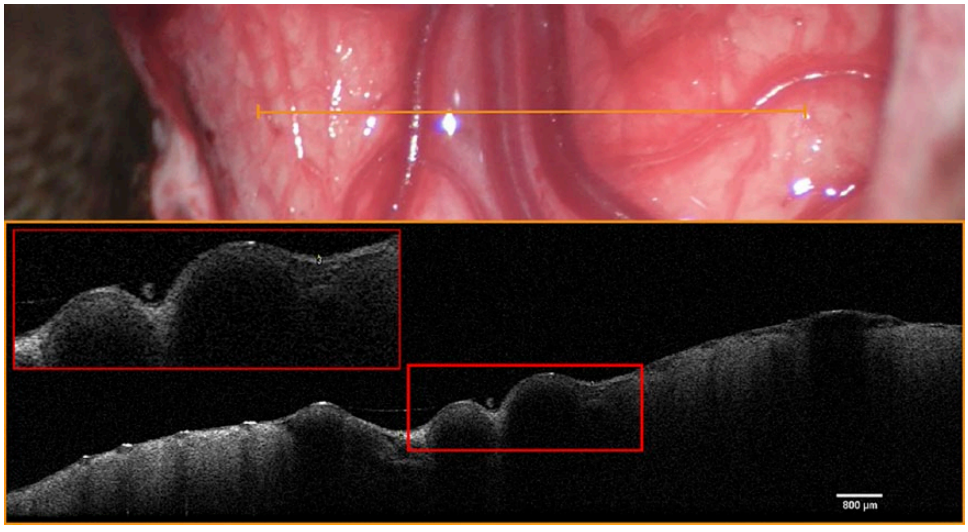

Figure 4. Above light microscopic picture of the parietal lobe with SAH associated with the surgical procedure after CSF release. The orange line demonstrates the scanning site. Below OCT-Scan with depiction of perivascular SAS. The ABCM does not show a clear differentiation to the trabecular system, internal blood vessels and brain cortex. Red rectangle shows enlarged details of the OCT-Scan.
CSF, cerebrospinal fluid; OCT, optical coherence tomography; SAH, subarachnoid haemorrhage.

The ABCM showed a mean depth of 81 µm frontotemporal, 46 µm frontal and 119 µm temporal (Figure 7). The ABCM at the sylvian fissure showed a higher depth (Figure 8).

Discussion

Ultrasound based methods-based methods are the gold standard for *in vivo* dynamic sectional imaging of the central nervous system, but lack

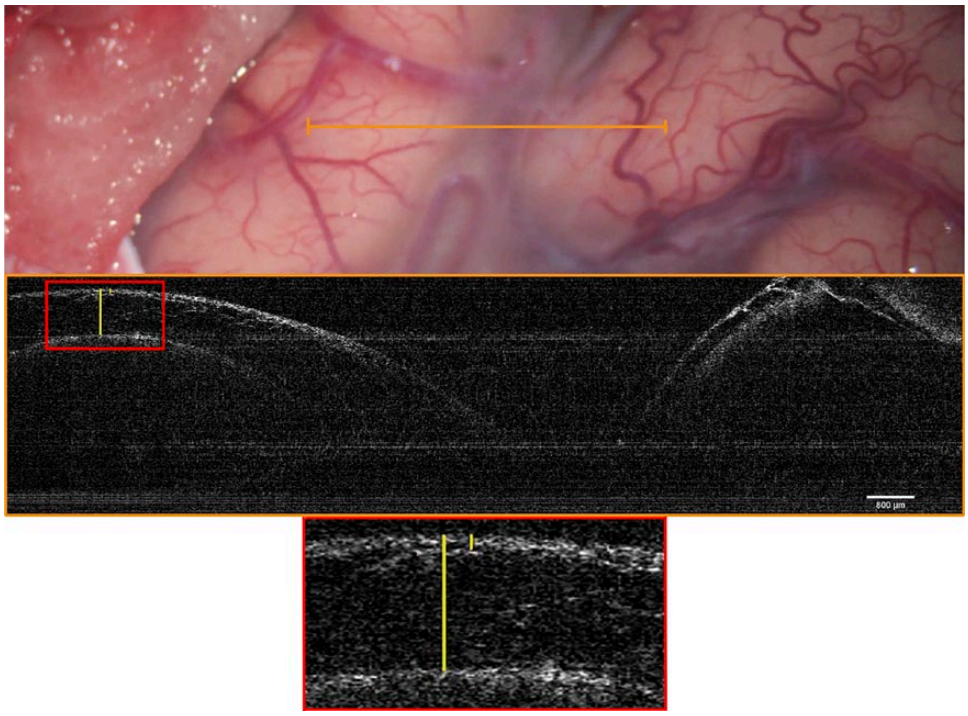

Figure 5. Above light microscopic picture of the frontal lobe. The horizontal orange line demonstrates the scanning site. Below OCT-scan of corresponding region. The red rectangle shows enlarged details of the OCT-Scan and demonstrates the measurement technique. The vertical yellow line indicates the measurement site of the depth of the SAS and the ABCM.
ABCM, arachnoid barrier cell membrane; OCT, optical coherence tomography; SAS, subarachnoid space.

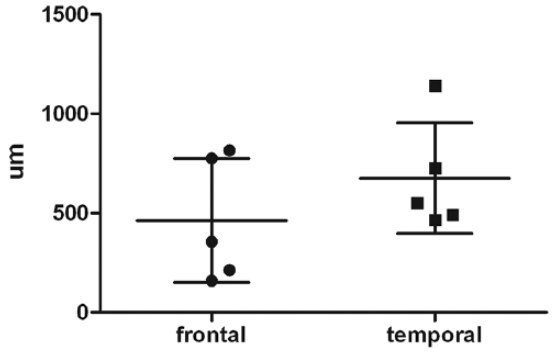

Figure 6. Depth of the frontal and temporal SAS.
SAS, subarachnoid space.

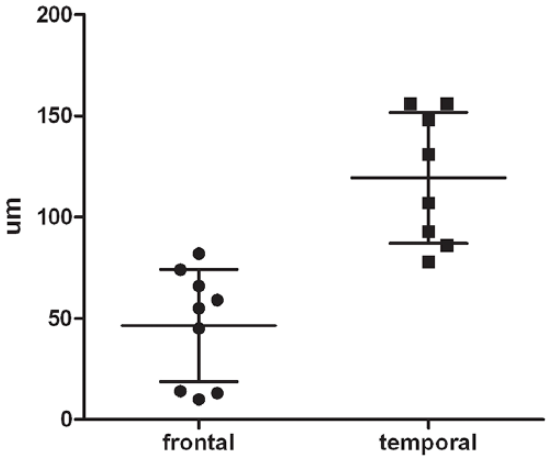

Figure 7. Depth of the frontal and temporal ABCM.
ABCM, arachnoid barrier cell membrane.

the spatial resolution to delineate the microstructural composition of the SAS.[2–4] Still imaging modalities are needed to display intact tissue and pathological alterations in the context of observational research and as intraoperative imaging tools. The present study reveals that microscope-integrated OCT might be capable of closing this neuroimaging gap. In addition, the technique showed to be a valuable tool for the first orthograde distance measurements of microanatomical structures of the SAS.

Albeit, *in vivo* conditions are constrained by tissue movements of several millimetres in amplitude which follow the respiratory and arterial cycle.[16] Microscope-integrated OCT offered a feasible

Figure 8. Above light microscopic image of the sylvian fissure. The horizontal orange line demonstrates the scanning site. Below OCT-Scan demonstrating the higher depth of the ABCM at the sylvian fissure.
ABCM, arachnoid barrier cell membrane.

technique to display the architecture of the intact SAS approaching the spatial resolution of histological analysis. Delineation of the ABCM, trabecula system, internal blood vessels and human brain cortex was robust, whereas differentiation of the pia mater was only possible in 26.9% of cases. Furthermore, SAH as a pathological condition could be clearly depicted. We demonstrated that SAH inhibited the delineation of trabeculae, ABCM, pia mater or minor internal blood vessels. The only prior study examining the SAS composition with OCT was carried out in CSF-released porcine brain *ex vivo* and reported a similar depiction of the ABCM, trabecular system, internal blood vessels and brain cortex, whereas differentiation of the pia mater was not possible. Post mortem conditions and CSF release with a collapsed SAS could here merely provide intragyral scanning.[19] Our data set demonstrated that under CSF-released conditions, in comparison with intact tissue, a clear differentiation between the ABCM and trabecular system was not possible; on the contrary ABCM depth could easily be overestimated by clinging trabeculae. CSF release furthermore, led to blood vessels which were adjacent to the human brain cortex. This resulted in pronounced optic shadows (Figure 3). Clinging as opposed to free trabeculae might minimize scattered radiation, enhancing optical density. In this respect, future experiments are necessary for clarification.

In animal studies, OCT recently proved to be a valuable and diverse neurophysiological imaging tool in domains like haemodynamic imaging,[24–27] functional imaging[28,29] and molecular imaging.[30] In experimental setups OCT could not only differentiate grey and white matter[12] but furthermore, healthy and tumor-invaded brain tissue.[16] These experimental results could be translated to intraoperative imaging *in vivo*.[17,18] Our mere delineation of the intact microanatomical architecture of the human SAS *in vivo* and the knowledge of the above mentioned optic effects are valuable state planning criteria for such conceivable future applications in clinical settings.

Microscope-integrated OCT offered the possibility for depth measuring of the human SAS *in vivo*. For the first time, depth measurements of these anatomical structures were possible. Technical accuracy was defined to 7.5µm. Due to the small number of participants, conditions after craniotomy with dural opening and the presence of brain-related pathologies, our results need reevaluation to define matters like age or sex which might influence the depth of these structures. As anatomically expected, we could demonstrate higher SAS depths at the level of the Sylvian fissure in relation to the frontotemporal SAS. Unexpectedly, we could demonstrate higher depths of the ABCM at the Sylvian fissure in comparison with the frontotemporal ABCM depth.

In previous studies, OCT showed a remarkable axial spatial resolution.[18] Since it depends on light, image acquisition is rapid and versatile implementations *via* fibre optic catheters are

simple.[31] In our study, we demonstrated that OCT offered a clear and robust delineation of the microanatomical composition of the intact human SAS and adjacent brain cortex. Further studies are necessary to evaluate the clinical relevance as an additional intraoperative tool during microsurgical procedures.

Acknowledgements

The authors thank M. Krug, CEO of OptoMedical Technologies GmbH, for valuable comments on the data analysis.

Funding

This research received no specific grant from any funding agency in the public, commercial, or not-for-profit sectors.

Conflict of interest statement

The authors have nothing to disclose. OptoMedical Technologies GmbH supported the study with free equipment for iOCT.

Supplemental material

Supplemental material for this article is available online.

ORCID iD

Karl Hartmann https://orcid.org/0000-0001-6732-952X

References

1. Yotsumoto Y and Watanabe T. Defining a link between perceptual learning and attention. *PLoS Biol* 2008; 6: e221.
2. van Velthoven V. Intraoperative ultrasound imaging: comparison of pathomorphological findings in US versus CT, MRI and intraoperative findings. In: *Intraoperative imaging in neurosurgery*. Vienna: Springer Vienna, 2003, pp. 95–99.
3. Unsgård G, Solheim O and Selbekk T. Intraoperative ultrasound in neurosurgery. In: *Intraoperative imaging and image-guided therapy*. New York, NY: Springer New York, 2014, pp. 549–565.
4. Vetrano IG and Prada F. Intraoperative findings in spinal lesions. In: *Intraoperative ultrasound (IOUS) in neurosurgery*. Cham: Springer International Publishing, 2016, pp. 59–69.
5. Ellerbee AK. *Optical coherence tomography: technology and applications*. New York: IEEE, 2014, pp. 7–8.
6. Beaurepaire E, Moreaux L, Amblard F, *et al.* Combined scanning optical coherence and two-photon-excited fluorescence microscopy. *Opt Lett* 1999; 24: 969–971.
7. Hee MR. Optical coherence tomography of the human retina. *Arch Ophthalmol* 1995; 113: 325–332.
8. Williams ZY, Schuman JS, Gamell L, *et al.* Optical coherence tomography measurement of nerve fiber layer thickness and the likelihood of a visual field defect. *Am J Ophthalmol* 2002; 134: 538–546.
9. Izatt J. *Intraoperative OCT for vitreoretinal surgery*. Washington, DC: OSA, 2012, p. BTu2B.1.
10. Valdés PA, Roberts DW, Lu F-K, *et al.* Optical technologies for intraoperative neurosurgical guidance. *Neurosurg Focus* 2016; 40: E8.
11. Janiszewska D. Cataract, refractive and glaucoma surgery: anterior eye segment photo, clinical details, TD OCT, SD OCT and SS OCT scans, diagnosis and conclusion. *Acta Ophthalmologica* 2010; 88. https://doi.org/10.1111/j.1755-3768.2010.1315.x
12. Nakaji H, Kouyama N, Muragaki Y, *et al.* Localization of nerve fiber bundles by polarization-sensitive optical coherence tomography. *J Neurosci Methods* 2008; 174: 82–90.
13. Axer M, Amunts K, Grässel D, *et al.* A novel approach to the human connectome: ultra-high-resolution mapping of fiber tracts in the brain. *NeuroImage* 2011; 54: 1091–1101.
14. Tearney GJ, Brezinski ME, Southern JF, *et al.* Optical biopsy in human urologic tissue using optical coherence tomography. *J Urol* 1997; 157: 1915–1919.
15. Fujimoto JG, Pitris C, Boppart SA, *et al.* Optical coherence tomography: an emerging technology for biomedical imaging and optical biopsy. *Neoplasia* 2000; 2: 9–25.
16. Böhringer HJ, Lankenau E, Stellmacher F, *et al.* Imaging of human brain tumor tissue by near-infrared laser coherence tomography. *Acta Neurochir (Wien)* 2009; 151: 507–517; discussion 517.
17. Kut C, Chaichana KL, Xi J, *et al.* Detection of human brain cancer infiltration ex vivo and in vivo using quantitative optical coherence tomography. *Sci Transl Med* 2015; 7: 292ra100.
18. Giese A, Böhringer HJ, Leppert J, Kantelhardt SR, Lankenau E, Koch P, et al. Non-invasive intraoperative optical coherence tomography of the resection cavity during surgery of

intrinsic brain tumors. Photonic Therapeutics and Diagnostics II. International Society for Optics and Photonics; SPIE Proceedings; 6078: 60782Z.

19. Scott G and Coats B. Microstructural characterization of the pia-arachnoid complex using optical coherence tomography. *IEEE Trans Med Imaging* 2015; 34: 1452–1459.
20. Drexler W. Enhanced visualization of macular pathology with the use of ultrahigh-resolution optical coherence tomography. *Arch Ophthalmol* 2003; 121: 695–706.
21. Gallwas J, Jalilova A, Ladurner R, *et al*. Detection of cervical intraepithelial neoplasia by using optical coherence tomography in combination with microscopy. *J Biomed Opt* 2017; 22: 16013.
22. Rueden CT, Schindelin J, Hiner MC, *et al*. ImageJ2: ImageJ for the next generation of scientific image data. *BMC Bioinformatics* 2017; 18: 529.
23. Schindelin J, Arganda-Carreras I, Frise E, *et al*. Fiji: an open-source platform for biological-image analysis. *Nat Methods* 2012; 9: 676–682.
24. Davis AM, Izatt JA and Tao YK. Single-pass volumetric bidirectional blood flow imaging spectral domain optical coherence tomography using a modified Hilbert transform. *Opt Express* 2008; 16: 12350–12361.
25. Skala MC, Crow MJ, Wax A, *et al*. Photothermal optical coherence tomography of epidermal growth factor receptor in live cells using immunotargeted gold nanospheres. *Nano Lett* 2008; 8: 3461–3467.
26. Faber DJ and van Leeuwen TG. Are quantitative attenuation measurements of blood by optical coherence tomography feasible? *Opt Lett* 2009; 34: 1435–1437.
27. Aguirre AD, Chen Y, Fujimoto JG, *et al*. Depth-resolved imaging of functional activation in the rat cerebral cortex using optical coherence tomography. *Opt Lett* 2006; 31: 3459–3461.
28. Eberle M. In vivo detection of cortical optical changes associated with seizure activity with optical coherence tomography. *Biomed Opt Express* 2012: 3: 2700–2706.
29. Tsytsarev V, Rao B, Maslov KI, *et al*. Photoacoustic and optical coherence tomography of epilepsy with high temporal and spatial resolution and dual optical contrasts. *J Neurosci Methods* 2013; 216: 142–145.
30. Skala MC, Tao YK, Davis AM, *et al.* (2011). Functional optical coherence tomography in preclinical models. In: Boas, David A., Constantinos, Pitris, and Nimmi, Ramanujam, eds. *Handbook of Biomedical Optics*. CRC press, 2016, pp.1–47.
31. Boppart SA. Optical coherence tomography: technology and applications for neuroimaging. *Psychophysiology* 2003; 40: 529–541.